

PLANETARY SCIENCE

Olivine alteration and the loss of Mars' early atmospheric carbon

Joshua Murray* and Oliver Jagoutz

The early Martian atmosphere had 0.25 to 4 bar of CO₂ but thinned rapidly around 3.5 billion years ago. The fate of that carbon remains poorly constrained. The hydrothermal alteration of ultramafic rocks, rich in Fe(II) and Mg, forms both abiotic methane, serpentine, and high-surface-area smectite clays. Given the abundance of ultramafic rocks and smectite in the Martian upper crust and the growing evidence of organic carbon in Martian sedimentary rocks, we quantify the effects of ultramafic alteration on the carbon cycle of early Mars. We calculate the capacity of Noachian-age clays to store organic carbon. Up to 1.7 bar of CO₂ can plausibly be adsorbed on clay surfaces. Coupling abiotic methanogenesis with best estimates of Mars' δ¹³C history predicts a reservoir of 0.6 to 1.3 bar of CO₂ equivalent. Such a reservoir could be used as an energy source for long-term missions. Our results further illustrate the control of water-rock reactions on the atmospheric evolution of planets.

INTRODUCTION

Geological observations of Mars indicate a dense early atmosphere ranging from 0.25 to 4 bar of CO₂ (1, 2). However, Mars' current surface reservoir only amounts to approximately 0.054 bar of CO₂, suggesting a substantial loss of CO₂, either to space or the lithosphere (3). This decline of CO₂ likely occurred between the late Noachian and late Hesperian period, when sedimentary deposits reflect a transition from a “warm and wet” to a “cold and dry” climate (1). The mechanism by which Mars lost its atmospheric CO₂ remains poorly constrained.

Photochemical models and orbiter measurements of carbon loss to space indicate an integrated escape since the Noachian of ~1.3 to 6.3 mbar of CO₂; two orders of magnitude lower than the rates necessary to explain the removal of 0.25 to 4 bar [(4, 5); see fig. S1]. Escape rates may have been amplified by an early magnetic dipole (6) and/or more frequent solar storms (7). In addition, sizeable amounts of CO₂ may have been sequestered as carbonate minerals (3); however, these large deposits have yet to be located (8). The challenge in reconciling models of Martian atmospheric evolution with present-day observations often leads to the postulation of a “missing sink” of carbon (8, 9).

Recent rover missions detected reduced organic carbon in Martian rocks (10–12). On Earth, reduced carbon species, primarily methane, are formed abiotically during low-temperature (<140°C) serpentinization (13). The oxidation of Fe(II) in olivine to Fe(III) in serpentine, which is abundant in ultramafic terrains on Mars (14, 15) and found as detrital minerals within deltaic sediments (16), liberates H₂ from water. Through the Sabatier reaction, this H₂ reacts with CO₂ to form methane, CH₄ (simplified in Eq. 1). Similar Fischer-Tropsch-type reactions can produce less reduced or more complex organic molecules and hydrocarbons (17, 18). Methane is unstable in the Martian atmosphere and would revert to CO₂ in less than 1 thousand years (ka) (19, 20) due to photochemical degradation (21).

However, smectite clays, the most abundant hydrated mineral on the Martian surface (22), have the capacity to adsorb and protect organic carbon (23, 24). Similar to serpentine, these clay minerals

form through water-rock reactions and alteration of mafic and ultramafic rocks (25, 26). Smectite surfaces can catalyze the polymerization and aromatization of simple organic carbon compounds (27) to molecules similar to those detected by the Perseverance rover (12). On Earth, tectonic processes and biological activity recycle lithospheric carbon back to the atmosphere (23, 28). On Mars, where these processes are limited or absent (29), mineral protected organic carbon in the crust would remain stable over long geologic timescales. Consequently, relatively small fluxes [e.g., (30)] could accumulate large lithospheric stores of organic carbon.

Here, we evaluate the role of abiotic methanogenesis and subsequent storage of methane within smectite clays in the cooling of the Martian climate. We constrain this process through a simple mass-balance model of serpentinization, estimates of the volume of clays within the crust, and a model of the evolution of carbon isotopes since the early Noachian.

RESULTS

Methane formation and storage

Our model explores the oxidation of Fe(II), present in e.g., olivine, which was abundant on Mars through at least the early Hesperian (31, 32), to serpentine. Eq. 1 shows a simplified, idealized reaction



We explore serpentinization volumes of 0- to 2-km global equivalent layer (GEL), within the depth of hydrated minerals on Mars (33) and inferred serpentinization on Earth (15). Our calculations show that a 2-km GEL of serpentine reduces ~5 bar of atmospheric CO₂ to methane (fig. S2).

Clay minerals on Mars are exposed in craters as deep as 17 km (33). However, the total volume of clays remains an uncertainty. The hydrated crust stores anywhere from 16- (34) to 1350-m GEL of H₂O [(35); upper limit], equivalent to 27- to 2260-m GEL of clay minerals (Materials and Methods). Given the uncertainty, we compute the capacity of smectite clays to store organic carbon for various total volumes (Fig. 1 and Materials and Methods) and investigate the implications of organic carbon storage as a function of clay volume, including both the “best estimate” of 218- to 436-m GEL smectite and the “plausible range” from 117- to 1440-m GEL (35).

Massachusetts Institute of Technology, Cambridge, MA, USA.

*Corresponding author. Email: joshmurr@mit.edu

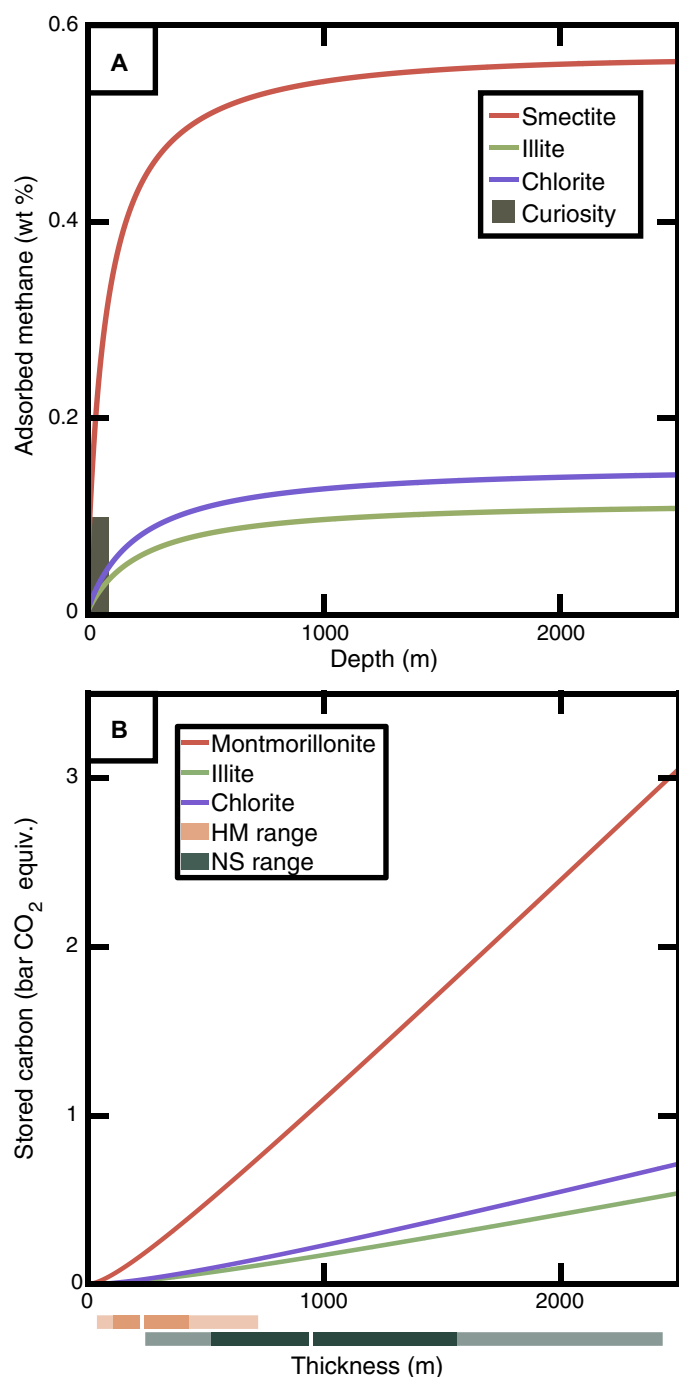


Fig. 1. Capacity for smectite clays to store organic carbon. (A) Calculations of adsorbed methane, shown as total organic carbon (TOC), on smectite, illite, and chlorite as a function of depth. Estimates are based on experimental data of Langmuir adsorption assuming an early Martian geotherm and crustal density (Materials and Methods). The gray bar shows the possible range of TOC in a mudstone sample in Gale crater (11). (B) Integrated TOC, converted to CO₂ atmospheric pressure, as a function of clay mineralogy and GEL thickness. The orange and green boxes reflect the one and two SD estimates of smectite clay volumes based on the formation of hydrated minerals (HM) and near-surface (NS) estimates, respectively [(35); Materials and Methods].

The methane storage capacity of different clay minerals is dependent on both pressure and temperature. Because of its high surface area, smectite can adsorb a factor of four more methane than illite or chlorite, with a maximum adsorption of ~0.6 weight % (wt %) (Fig. 1A and table S1). Integrating through the plausible volumes of smectite clay, our analysis indicates that 0.07 bar of CO₂ equivalent can be stored as methane within 117-m GEL and 1.7 bar in 1440-m GEL (Fig. 1B). The best-estimate clay volumes can store 0.16 to 0.4 bar of CO₂ as adsorbed methane. Compared to the nonpolar methane, smectite can store far greater percentages (up to 32 wt %) of polar molecules (36). Polar molecules are measured in Martian mudstones (10, 37) and can form abiotically in smectite interlayer spaces (27). In this regard, methane serves as a conservative estimate compared to the adsorption of possible compounds on clay surfaces. Below 500 m in depth, the maximum adsorbed methane concentration is relatively constant (Fig. 1A), indicating that the relationship between clay thickness and stored organic carbon is approximately linear (Fig. 1B). The depth distribution of the total clay volume is less influential: A 1000-m-thick surface layer of pure smectite can store 1.1 bar, whereas an equal volume distributed evenly throughout the upper 10 km can store 1.3 bar (fig. S3).

Our calculations show that Martian clays could store multiple bar of CO₂ equivalent. Reducing 1.7 bar of CO₂ to organic compounds would require ~700-m GEL depth of serpentinization (fig. S2). On Earth, the serpentinization of a 700-m-thick layer would take between 10 ka and 100 million years ago (Ma) (15). While serpentine is observed on Mars today (14), the extent of serpentinization could be obscured by subsequent alteration of serpentine to smectite since the Noachian (26).

Isotopic history

Abiotic methanogenesis preferentially incorporates light carbon isotopes (13). Consequently, the conversion of atmospheric CO₂ to mineral-bound CH₄ would lead to the fractionation of the carbon isotopic composition of the surface reservoir (Fig. 2). To model the change in isotopic composition of atmospheric CO₂ for varying GEL thicknesses of smectite clays and initial atmospheric pressure, we use a Monte Carlo method (Fig. 2 and Materials and Methods). We use a fractionation factor of $-14 \pm 3\%$ for methanogenesis, consistent with observations of abiotic systems on Earth [(13); Materials and Methods]. For the “lowest plausible” clay volume of 117-m GEL, we calculate an atmospheric enrichment of 0.4 to 1.8‰, depending on the initial atmospheric pressure of CO₂. The best estimate of clay volumes yields atmospheric enrichment in $\delta^{13}\text{C}$ of 1.9 to 14‰. The “highest plausible” volumes of 1440-m GEL stores 1.7 bar of CO₂ and would enrich $\delta^{13}\text{C}$ by 15 to 50‰, depending on the initial atmosphere (Fig. 2).

We place our predictions of $\delta^{13}\text{C}$ changes associated with methanogenesis within the constraints of the atmospheric evolution of carbon isotopes on Mars. Today, heavy carbon is strongly enriched, with atmospheric $\delta^{13}\text{C}$ measured as $48 \pm 4\%$ (38), while the early atmosphere likely reflected mantle $\delta^{13}\text{C}$ values of -30 to -20% (3, 39). Enriching atmospheric $\delta^{13}\text{C}$ from mantle values to present-day levels necessitates an increase of up to ~80‰ over Mars’ history (Fig. 2B). This enrichment is attributed, at least partially, to atmospheric escape. We combine modeled fractionation factors for photodissociation of CO (3) with best estimates of atmospheric escape of atomic carbon (4) and project $\delta^{13}\text{C}$ back to the Noachian (see Materials and Methods; Fig. 2B). We find integrated atmospheric

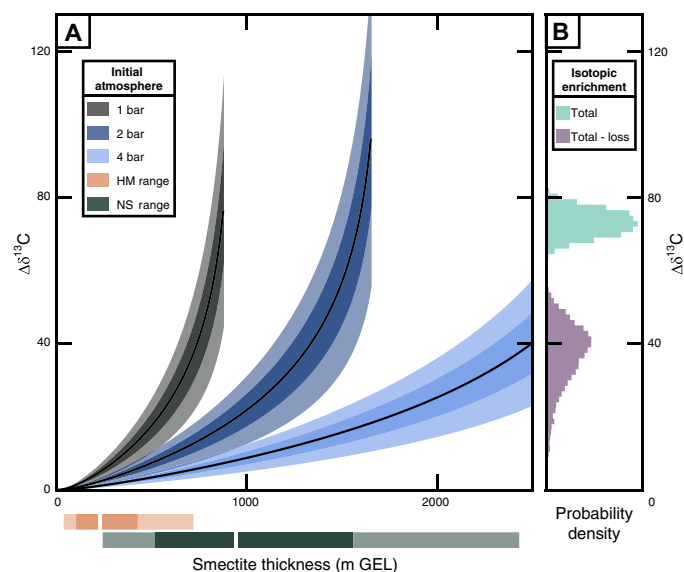


Fig. 2. Predicted change in atmospheric $\delta^{13}\text{C}$ for a variable volume of smectite clays saturated with abiotic methane. (A) Colored segments reflect different initial Martian atmospheric pressures. Data are shown with median (black line), 1 SD (near-opaque field), and 2 SDs (semitransparent field). The orange and green boxes reflect the one and two standard deviation estimates of smectite clay thickness as shown in Fig. 1. (B) Probability density of changes in $\delta^{13}\text{C}$ for the total enrichment since 4.5 Ga (turquoise) and the total enrichment that cannot be explained by current estimates of atmospheric loss alone (purple).

loss since 4.0 Ga can account for 34^{+11}_{-6} ‰ of isotopic enrichment (Fig. 2B). The remaining 38^{+7}_{-11} ‰ of enrichment must be attributable to a process not included in these integrated estimates of loss to space. Loss rates could be substantially greater in the past (6, 7), particularly if oxygen escape is derived from CO_2 photodissociation rather than H_2O (40). However, modern loss rates of carbon are ~ 2 orders of magnitude lower than oxygen loss rates (5, 40), and enhanced loss in the early solar system is difficult to quantify, particularly if $\delta^{13}\text{C}$ enrichment is driven by a combination of geologic and atmospheric mechanisms.

Here, we explore the effect of abiotic methanogenesis on the history of $\delta^{13}\text{C}$ and consider the extent to which water-rock reactions can bridge the gap between early magmatic $\delta^{13}\text{C}$ values and the $\delta^{13}\text{C}$ inferred through the extrapolation of modern atmospheric loss (4). Figure 3 overlays the change in atmospheric $\delta^{13}\text{C}$ associated with various GEL thicknesses of organic matter bearing smectite clay, for an initial 2 bar of CO_2 atmosphere. Subsequently, we evaluate the size of organic reservoir, formed by abiotic methanogenesis, required to explain the isotopic discrepancy (Fig. 2B).

To do so, we use a Bayesian treatment of clay volumes, isotopic fractionation, initial $\delta^{13}\text{C}$, and present conditions to calculate the conditional probability distribution of organic carbon in the Martian crust given the isotopic composition of the atmosphere at 4 Ga (Materials and Methods). For an initial atmospheric CO_2 pressure of 1 bar, an organic carbon reservoir equivalent to $0.65^{+0.15}_{-0.30}$ bar of CO_2 best recreates the available data (Fig. 4). An initial atmospheric pressure of 2 bar is best fit by an organic carbon reservoir equivalent to $1.25^{+0.29}_{-0.69}$ bar of CO_2 . These organic carbon reservoirs equate to total masses of 0.69 to 1.33 PT of carbon. To reduce

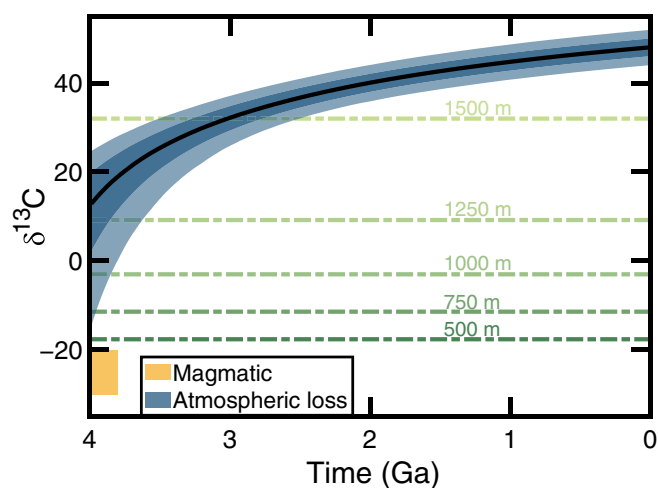


Fig. 3. Enrichment of Martian $\delta^{13}\text{C}$ since 4.0 Ga due to atmospheric escape and volume-dependent enrichment by mineral-bound organic carbon. The blue field is calculated by projecting the modern atmospheric composition backwards with best estimates of photodissociation and solar evolution [(4, 62); Materials and Methods]. The median, 1 SD, and 2 SDs are displayed as the black line, near-opaque field, and semitransparent field, respectively. The magmatic composition of Martian meteorites is shown as a yellow bar (39). Green dashed lines show the median $\delta^{13}\text{C}$ predicted by smectite clays of various GEL thicknesses for an initial atmosphere of 2 bar of CO_2 . See fig. S4 for a comparable figure with other loss estimates and initial atmospheric pressures.

that amount of carbon requires at least 280- to 510-m GEL of serpentinization (fig. S2) and at least 670- to 1100-m GEL of smectite to adsorb and protect the carbon in the crust (Fig. 1). For an initial atmosphere of 1 and 2 bar, respectively, we find that the mineral-bound organic carbon reservoir cannot exceed masses equivalent to 0.85 and 1.7 bar, else atmospheric $\delta^{13}\text{C}$ is enriched beyond modern values (Fig. 2). This corresponds to an upper limit in methane-saturated smectite clays of 800- and 1500-m GEL, respectively (Fig. 1B), consistent with the highest plausible limits derived from estimates of crustal H_2O (34, 35).

An initial atmosphere of 4 bar requires greater than 2-km GEL of smectite clay minerals and associated methane to recreate the isotopic enrichment observed today (Fig. 2 and fig. S5). Such a volume is beyond the plausible limit of hydrated minerals on Mars (35). If the early Martian atmosphere were as thick as 4 bar, then other processes, which either concentrates carbon within the crust beyond methane adsorption or markedly increase the rate of atmospheric escape (2), would be necessary to explain the loss of carbon.

In addition to carbon, hydrogen is fractionated during the formation of methane. Using a fractionation factor of $325 \pm 50\text{‰}$ [(10) and table S1], we estimate an enrichment in D/H of 0.01 to 0.4 Vienna Standard Mean Ocean Water (VSMOW), depending on the initial atmospheric pressure of CO_2 and the size of the water reservoir at 4 Ga (fig. S9). An enrichment of 0.4 VSMOW is minor in comparison to the ~ 5 VSMOW enrichment in D/H since the Noachian, which was driven largely by atmospheric escape (38, 41). The large uncertainties in hydrogen escape rates through time—including the dependency on solar extreme ultraviolet (42), the effect of dust storms (43, 44), and the changes in orbital obliquity (45)—pose a barrier to relating abiotic methanogenesis to the history of

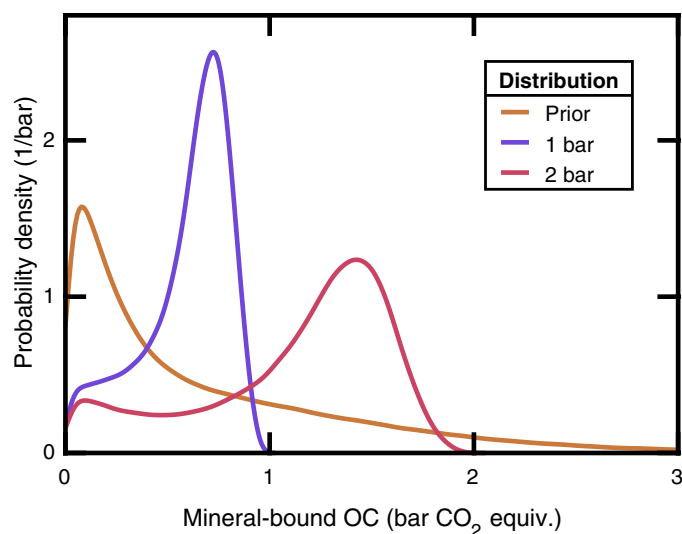


Fig. 4. Prior and posterior probability distributions of organic carbon in the Martian crust. The prior distribution (orange line) is calculated according to the combined near-surface and hydrated mineral estimates of H₂O in the Martian crust [(35); Materials and Methods] and converted to organic carbon by the calculations shown in Fig. 1B. Posterior distributions are conditional upon an initial 1 bar of atmosphere (purple line) and an initial 2 bar of atmosphere (red line). Posterior distributions reflect the organic carbon reservoir required to replicate $\delta^{13}\text{C}$ predicted by atmospheric escape models. Comparable figures are presented in the Supplementary Materials with prior distributions derived solely from near-surface estimates and hydrated mineral formation (figs. S6 and S7).

Martian D/H. Because of these uncertainties, we refrain from using D/H as a constraint to infer the size of the organic carbon reservoir. Future models of Martian D/H may benefit from the inclusion of abiotic methanogenesis but only if loss-driven hydrogen fractionation through time is known to greater precision than ~ 0.5 VSMOW.

DISCUSSION

Our results demonstrate that serpentinization indeed could have formed a large organic carbon reservoir due to the reduction of atmospheric CO₂. This reservoir, stored and protected on clay mineral surfaces since the Noachian, could represent the postulated missing sink of carbon on Mars. We demonstrate that Mars' climatic and carbon isotopic history can be explained with the inclusion of an organic carbon reservoir equivalent to ~ 0.4 to 1.5 bar of CO₂. Given that we do not attempt to model the effects of an early magnetic field and solar storms, our integrated loss estimates likely reflect a lower bound [(4) and Materials and Methods]. It follows that the size of the organic carbon reservoir is an upper bound. The $\delta^{13}\text{C}$ enrichment (Fig. 2B) can thus be partitioned between the storage of organic molecules on clay surfaces (this paper) and unquantified processes, which enhance the loss to space of CO₂.

The bounds placed on the organic carbon reservoir could be further constrained by measurements of organic carbon within Martian mudstones, particularly in the subsurface, to investigate the depth dependence predicted in Fig. 1A. On Earth, we can garner greater understanding through study of abiotic methanogenesis in serpentinites of compositions more similar to those on Mars (15) and through laboratory measurements that constrain isotopic

fractionation during the formation of complex organic molecules within the interlayer space of smectites (27).

Traditionally, 2 wt % TOC is seen as a minimum for economical extraction of gas from shale (46). However, space exploration need not be profitable, and 0.5 wt % could provide a valuable fuel source. If extracted, Martian organic carbon, particularly methane, could be used as a propellant for farther space missions or return flights (47, 48). Alternatively, methane and hydrogen act as potent greenhouse gases in the Martian atmosphere (49) and could be used more effectively for terraforming than other accessible carbon reservoirs (50). Processes that further concentrate organic carbon in shales or in traps would make these ventures more achievable and justifies searching for concentrated deposits in the subsurface.

Our results may have ramifications beyond Mars' climate history. Given that tectonic processes have overturned and obscured most Hadean and Archaean crust on Earth, Mars provides the best window into planetary processes in the ~ 1 billion years after accretion. Our results show that aqueous alteration and serpentinization of (ultra-) mafic rocks are critical processes for the exchange of hydrogen and carbon between the ocean-atmosphere and the lithosphere and can meaningfully influence the CO₂ budget of a planet's atmosphere. Our model of abiotic methanogenesis and storage, shown in the schematic Fig. 5, which is minor on Earth today, may be a widespread, fundamental process in the atmospheric evolution of young rocky planets with an (ultra-) mafic crust. The formation and adsorption of organic molecules formed soon after planetary accretion could even be integral to the development of life (27, 51). However, in the absence of tectonic overturning of the crust, the adsorption of organic carbon onto clay surfaces may represent an irreversible loss of atmospheric carbon, further tying plate tectonics to planetary habitability even in the absence of substantial carbonate deposits (52).

MATERIALS AND METHODS

Abiotic methanogenesis

To investigate the relationship between abiotic methanogenesis and serpentinization volume, we assume that reactant olivine has a

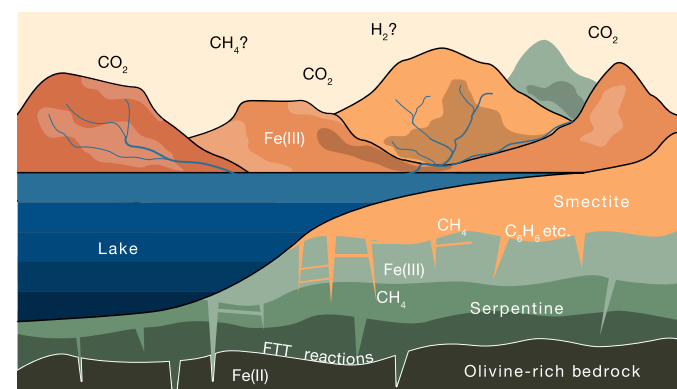


Fig. 5. Schematic for our framework of organic carbon sequestration on early Mars. Ultramafic rocks are hydrothermally altered in the subsurface to form serpentine, smectite, and methane. Methane is adsorbed in the smectite interlayer space, where it may further react to form complex organic molecules (27). When combined, these reactions amass geologically significant stores of carbon within the crust. FTT, Fischer-Tropsch type.

forsterite number of 0.6 and an Fe(II)/ΣFe of 1 (53). We use a forsterite density of 3300 kg/m³ and a fayalite density of 4400 kg/m³. We model olivine alteration to serpentine with a final Fe(II)/ΣFe of 0.4 (15). We explore GEL depths of 0 to 2 km, consistent with 1 billion years ago (Ga) of the slowest estimates of the migration of serpentinization reaction fronts (15). If serpentine is a precursor to the hydrated minerals observed on Mars (26), then the 2-km GEL is the upper limit of total serpentinization; however, magnetic data may suggest substantially greater depths (15).

We follow the chemical equation of (54) in which 6 mol of fayalite form 1 mol of methane. GEL thicknesses of serpentinization are then converted to mol of olivine, mol of methane, and lastly atmospheric pressure of CO₂ (fig. S1).

Methane adsorption

The adsorption of methane on clay surfaces is dependent on mineralogy, pressure, and temperature. We assume an upper crustal density of 3100 kg/m³ (55, 56), a clay density of 2300 kg/m³, a surface temperature of 0°C, and a Martian geotherm of 15 K/km (57). We convert depth to temperature and calculate the Langmuir coefficient, K , according to (58)

$$\ln(K) = \frac{q}{RT} + \frac{\Delta S^0}{R} - \ln(p^0) \quad (2)$$

where q is the heat of adsorption; ΔS^0 is the standard entropy of adsorption, R is the gas constant, T is temperature, and (p^0) is the standard pressure, 1 bar.

We then calculate the adsorption of methane, Γ , according to the Langmuir coefficient

$$\Gamma = \Gamma_{\max} \frac{K \cdot P}{K \cdot P + 1} \quad (3)$$

For smectite, illite, and chlorite, the values of q , ΔS^0 , and Γ_{\max} are given in table S1 (58). We use numerical integration of Γ with depth to derive the total adsorption of methane for a given thickness of smectite (Fig. 1B).

Clay volumes

The total volume of clay minerals in the Martian crust is a major control to the history of water on Mars; however, constraining clay abundance and water content at depth remains challenging (34, 35, 57). We derive our range of smectite volumes from two existing estimates of water sequestered in the crust: The first is constrained by the H₂O necessary to form hydrated minerals; the second is constrained by estimates of H₂O in the near surface of Mars (35). The prior distribution for our inferred reservoir of organic carbon is evenly sampled from the hydrated mineral distribution and near-surface distribution [(35); Fig. 4], and we present the results for each distribution separately within the Supplementary Materials (figs. S6 and S7).

The majority (62%) of detected hydrated minerals on Mars are smectite clays (35). A further 23% are chlorite (35), which is formed primarily by the diagenetic alteration of smectite (22). Adsorbed organic matter is retained during the diagenesis of smectite (59). Hence, we assume that 85% of hydrated minerals in the Martian crust were smectite clays or remain as smectite clays. We convert mineral-bound H₂O estimates to GEL thickness of smectite clay assuming a water content of 22 wt % and a density of 2300 kg/m³. This results in a conversion factor of 1.68 from H₂O (m GEL) to smectite

clay (m GEL) (see fig. S8) for a comparison. The “plausible” range of water sequestered within the crust, 70- to 860-m GEL (35), is thus equivalent to 117- to 1440-m GEL of smectite clay.

Isotopic fractionation during abiotic methanogenesis

We use a Monte Carlo method to randomly sample the fractionation factor of abiotic methanogenesis and model the subsequent isotopic enrichment of ¹³C in the atmosphere. We generate a fractionation factor according to the normal distribution $-14 \pm 3\%$ (table S1). Distinguishing biotic and abiotic methane signatures on Earth is challenging; however, biotic methane tends to have a lighter signature than abiotic methane (although both processes preferentially incorporate ¹²C). The range $-14 \pm 3\%$ is chosen to reflect the majority of samples studied in the Semail and Al Farfar ophiolites (13), as well as the abiotic methane catalyzed by chromium spinel (60), which is detected in Jezero Crater (16).

As methane reacts within the smectite interlayer space to form more complex organic compounds, carbon may be fractionated again. If some of the organic carbon were then freed to the atmosphere, then the fractionation during complex abiotic polymerization and aromatization reactions would play a role in the atmospheric evolution of $\delta^{13}\text{C}$. These reactions have not been well-studied from an isotopic standpoint and remain a source of uncertainty in our model. We suggest that, given the tendency for abiotic ethane to incorporate more ¹²C than does abiotic methane (13, 60), our fractionation factors are more likely to underestimate the strength of fractionation than overestimate. Similarly, abiotic methanogenesis tends to incorporate more ¹²C at lower temperatures (61). Given a cooler Martian geotherm and surface temperatures, serpentinization on Noachian Mars may have fractionated carbon more strongly than modern ophiolite complexes.

To calculate the change in $\delta^{13}\text{C}$ of the atmosphere, we run simulations with a given starting atmospheric pressure of CO₂ and a global thickness of smectite clays. We then calculate the ratio of carbon, which could be sequestered as mineral-bound methane, relative to the starting atmospheric carbon. We use this ratio of sequestered carbon and the fractionation factor discussed above to calculate change in atmospheric $\delta^{13}\text{C}$ by the Rayleigh equation (Fig. 2).

We use the same methodology to calculate the influence of abiotic methanogenic on hydrogen isotopes. We use a D/H range of $-325 \pm 50\%$ for abiotic methane, relative to the source H₂O (13). The resulting change in atmospheric D/H is shown in fig. S9.

Atmospheric escape and $\delta^{13}\text{C}$

Estimates of atmospheric escape can be derived via multiple methods. The loss of O to space, as measured by MAVEN [e.g., (42)], can be tied to CO₂ photodissociation but may be derived primarily from the photodissociation of H₂O (2, 9). Alternatively, the isotopic fractionation since the Noachian has been used to estimate the amount of CO₂ loss, assuming a fractionation factor for photodissociation of CO (3). However, the mechanism of carbon loss outlined here also enriches carbon isotopes in the atmosphere, so we cannot use modern $\delta^{13}\text{C}$ to constrain both methanogenesis and atmospheric loss. Instead, we use recently calculated total modern loss rates that include photodissociation, dissociative recombination, electron impact dissociation, and photoionization (4). We scale the total modern loss with the intensity of the solar Lyman continuum (Eq. 4) (4, 62). The relationship between the flux of photons in the Lyman

continuum and the photodissociation of CO₂ is unknown (3). We assume a power law with an exponent sampled from a lognormal distribution with mean 1.5 and standard deviation 0.25.

$$F_c = [F_0(4.5 - t)^{\beta_{\text{lym}}}]^{\alpha_{\text{lym}}} \quad (4)$$

We apply a total carbon isotope fractionation factor of 0.6, which is calculated specifically for photodissociation of CO (3). We project loss rates backward from the present to 4 Ga, adding carbon back into the atmosphere and tracking the resultant $\delta^{13}\text{C}$.

A full set of model parameters is given in table S1. In the Supplementary Materials, we provide an alternative history of $\delta^{13}\text{C}$ using the ion loss rates from solar wind-driven ion escape, constrained by the Mars Express orbiter [(5); fig. S4].

Inference of the organic carbon reservoir

Assuming that abiotic methanogenesis is responsible for the previously unaccounted enrichment in ^{13}C , we can put estimates on the amount of organic carbon stored in Martian clays.

Once again, we use Monte Carlo simulations to generate two separate distributions of $\delta^{13}\text{C}$: the first from mineral-bound abiotic methane and the second from rewinding 4 Ga of atmospheric loss. Our prior distribution for methane-driven $\delta^{13}\text{C}$ is derived from the estimated probability distribution of water in hydrated minerals on Mars [figure 4 of (35)] converted to clay volume. We then use Bayes theorem to calculate the posterior distribution of mineral-bound organic carbon according to the likelihood (the probability distribution of $\delta^{13}\text{C}$ at 4 Ga according to our model of atmospheric escape) and the prior (the probability distribution of $\delta^{13}\text{C}$ beginning from magmatic values and enriched by abiotic methanogenesis). We handle the probabilities numerically via weighted resampling with replacement of the parameters in the abiotic methanogenesis model.

For an initial atmosphere of 4 bar of CO₂, only 3% of simulations of methanogenesis exceed the $\delta^{13}\text{C}$ inferred from atmosphere escape i.e., for our framework to bridge the gap between magmatic values and modern values requires loss rates that are improbably high or fractionation factors for abiotic methanogenesis which are improbably low. Hence, we do not include the posterior distribution of mineral-bound organic carbon for a 4 bar atmosphere in Fig. 4 and suggest that another process would likely be necessary to remove such a large reservoir of carbon. For completeness, the posterior distribution is shown in fig. S5.

Supplementary Materials

This PDF file includes:

Table S1

Figs. S1 to S9

REFERENCES AND NOTES

1. E. S. Kite, Geologic constraints on early Mars climate. *Space Sci. Rev.* **215**, 1–47 (2019).
2. B. M. Jakosky, The CO₂ inventory on Mars. *Planet. Space Sci.* **175**, 52–59 (2019).
3. H. Renyu, D. M. Kass, B. L. Ehlmann, Y. L. Yung, Tracing the fate of carbon and the atmospheric evolution of Mars. *Nat. Commun.* **6**, 10003 (2015).
4. D. Y. Lo, R. V. Yelle, R. J. Lillis, J. I. Deighan, Carbon photochemical escape rates from the modern Mars atmosphere. *Icarus* **360**, 114371 (2021).
5. R. Ramstad, S. Barabash, Y. Futaana, H. Nilsson, M. Holmström, Ion escape from Mars through time: An extrapolation of atmospheric loss based on 10 years of Mars Express measurements. *J. Geophys. Res. Planets* **123**, 3051–3060 (2018).
6. S. Sakai, K. Seki, N. Terada, H. Shinagawa, T. Tanaka, Y. Ebihara, Effects of a weak intrinsic magnetic field on atmospheric escape from Mars. *Geophys. Res. Lett.* **45**, 9336–9343 (2018).
7. B. M. Jakosky, J. M. Grebowsky, J. G. Luhmann, J. Connerney, F. Eparvier, R. Ergun, J. Halekas, D. Larson, P. Mahaffy, J. McFadden, D. L. Mitchell, N. Schneider, R. Zurek, S. Bougher, D. Brain, Y. J. Ma, C. Mazelle, L. Andersson, D. Andrews, D. Baird, D. Baker, J. M. Bell, M. Benna, M. Chaffin, P. Chamberlin, Y.-Y. Chaufray, J. Clarke, G. Collinson, M. Combi, F. Crary, T. Cravens, M. Crismani, S. Curry, D. Curtis, J. Deighan, G. Delory, R. Dewey, G. DiBraccio, C. Dong, Y. Dong, P. Dunn, M. Elrod, S. England, A. Eriksson, J. Espley, S. Evans, X. Fang, M. Fillingim, K. Fortier, C. M. Fowler, J. Fox, H. Gröller, S. Guzewich, T. Hara, Y. Harada, G. Holsclaw, S. K. Jain, R. Jolitz, F. Leblanc, C. O. Lee, Y. Lee, F. Lefevre, R. Lillis, R. Livi, D. Lo, M. Mayyasi, W. McClintock, T. McNulty, M. Modolo, F. Montmessin, M. Morooka, A. Nagy, K. Olsen, W. Peterson, A. Rahmati, S. Ruhunusiri, C. T. Russell, S. Sakai, J.-A. Sauvaud, K. Seki, M. Steckiewicz, M. Stevens, A. I. F. Stewart, A. Stiepen, S. Stone, V. Tenishev, E. Thiemann, R. Tolson, D. Toublanc, M. Vogt, T. Weber, P. Withers, T. Woods, R. Yelle, MAVEN observations of the response of Mars to an interplanetary coronal mass ejection. *Science* **350**, aad0210 (2015).
8. C. S. Edwards, B. L. Ehlmann, Carbon sequestration on Mars. *Geology* **43**, 863–866 (2015).
9. A. W. Heard, E. S. Kite, A probabilistic case for a large missing carbon sink on Mars after 3.5 billion years ago. *Earth Planet. Sci. Lett.* **531**, 116001 (2020).
10. D. P. Glavin, C. Freissinet, K. E. Miller, J. L. Eigenbrode, A. E. Brunner, A. Buch, B. Sutter, P. D. Archer Jr., S. K. Atreya, W. B. Brinckerhoff, M. Cabane, P. Coll, P. G. Conrad, D. Coscia, J. P. Dworkin, H. B. Franz, J. P. Grotzinger, L. A. Leshin, M. G. Martin, C. McKay, D. W. Ming, R. Navarro-González, A. Pavlov, A. Steele, R. E. Summons, C. Szopa, S. Teinturier, P. R. Mahaffy, Evidence for perchlorates and the origin of chlorinated hydrocarbons detected by SAM at the Rocknest aeolian deposit in Gale Crater. *J. Geophys. Res. Planets* **118**, 1955–1973 (2013).
11. J. C. Stern, C. A. Malespin, J. L. Eigenbrode, C. R. Webster, G. Flesch, H. B. Franz, H. V. Graham, C. H. House, B. Sutter, P. D. Archer Jr., A. E. Hofmann, A. C. McAdam, D. W. Ming, R. Navarro-Gonzalez, A. Steele, C. Freissinet, P. R. Mahaffy, Organic carbon concentrations in 3.5-billion-year-old lacustrine mudstones of Mars. *Proc. Natl. Acad. Sci. U.S.A.* **119**, e2201139119 (2022).
12. S. Sharma, R. D. Roppel, A. E. Murphy, L. W. Beegle, R. Bhartia, A. Steele, J. R. Hollis, S. Siljeström, F. M. McCubbin, S. A. Asher, W. J. Abbey, A. C. Allwood, E. L. Berger, B. L. Bleefeld, A. S. Burton, S. V. Bykov, E. L. Cardarelli, P. G. Conrad, A. Corpolongo, A. D. Czaja, L. P. DeFlores, K. Edgett, K. A. Farley, T. Fornaro, A. C. Fox, M. D. Fries, D. Harker, K. Hickman-Lewis, J. Huggett, S. Imbeah, R. S. Jakubek, L. C. Kah, C. Lee, Y. Liu, A. Magee, M. Minitti, K. R. Moore, A. Pascuzzo, C. Rodriguez Sanchez-Vahamonde, E. L. Scheller, S. Shkolyar, K. M. Stack, K. Steadman, M. Tuite, K. Uckert, A. Werynski, R. C. Wiens, A. J. Williams, K. Winchell, M. R. Kennedy, A. Yanchilina, Diverse organic-mineral associations in Jezero crater, Mars. *Nature* **619**, 724–732 (2022).
13. G. Etiope, M. J. Whiticar, Abiotic methane in continental ultramafic rock systems: Towards a genetic model. *Appl. Geochem.* **102**, 139–152 (2019).
14. B. L. Ehlmann, J. F. Mustard, S. L. Murchie, Geologic setting of serpentine deposits on Mars. *Geophys. Res. Lett.* **37**, L06201 (2010).
15. B. M. Tutolo, N. J. Tosca, Observational constraints on the process and products of Martian serpentinization. *Sci. Adv.* **9**, eadd8472 (2023).
16. M. M. Tice, Joel A. Hurowitz, Kirsten L. Siebach, E. L. Moreland, T. V. Kizovski, Mariek E. Schmidt, L. P. O'Neil, A. H. Treiman, B. Clark, M. Jones, A. Allwood, M. L. Cable, G. Caravaca, S. Siljeström, N. Randazzo, J. I. Simon, Regional Paleoenvironments Recorded in Sedimentary Rocks of the Western Fan-Delta, Jezero Crater, Mars, in the 55th Lunar and Planetary Science Conference (2024).
17. A. Steele, L. G. Benning, R. Wirth, S. Siljeström, M. D. Fries, E. Hauri, P. G. Conrad, K. Rogers, J. Eigenbrode, A. Schreiber, A. Needham, J. H. Wang, F. M. McCubbin, D. Kilcoyne, J. D. R. Blanco, Organic synthesis on Mars by electrochemical reduction of CO₂. *Sci. Adv.* **4**, eaat5118 (2018).
18. M. E. Berndt, D. E. Allen, W. E. Seyfried Jr., Reduction of CO₂ during serpentinization of olivine at 300 C and 500 bar. *Geology* **24**, 351–354 (1996).
19. F. Lefevre, F. Forget, Observed variations of methane on Mars unexplained by known atmospheric chemistry and physics. *Nature* **460**, 720–723 (2009).
20. V. A. Krasnopolsky, J. P. Maillard, T. C. Owen, Detection of methane in the martian atmosphere: Evidence for life? *Icarus* **172**, 537–547 (2004).
21. A.-S. Wong, S. K. Atreya, T. Encrenaz, Chemical markers of possible hot spots on Mars. *J. Geophys. Res. Planets* **108**, 5026 (2003).
22. B. L. Ehlmann, J. F. Mustard, R. N. Clark, G. A. Swayze, S. L. Murchie, Evidence for low-grade metamorphism, hydrothermal alteration, and diagenesis on Mars from phyllosilicate mineral assemblages. *Clay Clay Miner.* **59**, 359–377 (2011).
23. J. I. Hedges, R. G. Keil, Sedimentary organic matter preservation: an assessment and speculative synthesis. *Mar. Chem.* **49**, 81–115 (1995).
24. J. Murray, O. Jagoutz, Palaeozoic cooling modulated by ophiolite weathering through organic carbon preservation. *Nat. Geosci.* **17**, 88–93 (2024).
25. W. E. Seyfried Jr., M. J. Mottl, Hydrothermal alteration of basalt by seawater under seawater-dominated conditions. *Geochim. Cosmochim. Acta* **46**, 985–1002 (1982).

26. J. Caillaud, D. Proust, D. Righi, Weathering sequences of rock-forming minerals in a serpentinite: influence of microsystems on clay mineralogy. *Clay Clay Miner.* **54**, 87–100 (2006).
27. L. B. Williams, B. Canfield, K. M. Voglesonger, J. R. Holloway, Organic molecules formed in a “primordial womb”. *Geology* **33**, 913–916 (2005).
28. P. B. Kelemen, C. E. Manning, Reevaluating carbon fluxes in subduction zones, what goes down, mostly comes up. *Proc. Natl. Acad. Sci. U.S.A.* **112**, E3997–E4006 (2015).
29. M. T. Zuber, The crust and mantle of Mars. *Nature* **412**, 220–227 (2001).
30. J. Krissansen-Totton, S. Olson, D. C. Catling, Disequilibrium biosignatures over Earth history and implications for detecting exoplanet life. *Sci. Adv.* **4**, eaao5747 (2018).
31. J. F. Mustard, F. Poulet, A. Gendrin, J. P. Bibring, V. Langevin, B. Gondet, N. Mangold, G. Bellucci, F. Altieri, Olivine and pyroxene diversity in the crust of Mars. *Science* **307**, 1594–1597 (2005).
32. B. L. Ehlmann, C. S. Edwards, Mineralogy of the Martian surface. *Annu. Rev. Earth Planet. Sci.* **42**, 291–315 (2014).
33. V. Z. Sun, R. E. Milliken, Ancient and recent clay formation on Mars as revealed from a global survey of hydrous minerals in crater central peaks. *J. Geophys. Res. Planets* **120**, 2293–2332 (2015).
34. J. F. Mustard, Sequestration of volatiles in the Martian crust through hydrated minerals: A significant planetary reservoir of water, *In Volatiles in the martian crust* (Elsevier, 2019), pp. 247–263.
35. L. J. Wernicke, B. M. Jakosky, Martian hydrated minerals: A significant water sink. *J. Geophys. Res. Planets* **126**, e2019JE006351 (2021).
36. Y.-H. Shen, Phenol sorption by organoclays having different charge characteristics. *Colloids Surf. A Physicochem. Eng. Asp.* **232**, 143–149 (2004).
37. J. L. Eigenbrode, R. E. Summons, A. Steele, C. Freissinet, M. Millan, R. Navarro-González, B. Sutter, A. McAdam, H. B. Franz, D. P. Glavin, P. D. Archer Jr., P. R. Mahaffy, P. G. Conrad, J. A. Hurowitz, J. P. Grotzinger, S. Gupta, D. W. Ming, D. Y. Sumner, C. Szopa, C. Malespin, A. Buch, P. Coll, Organic matter preserved in 3-billion-year-old mudstones at Gale crater. *Mars. Science* **360**, 1096–1101 (2018).
38. C. R. Webster, P. R. Mahaffy, G. J. Flesch, P. B. Niles, J. H. Jones, L. A. Leshin, S. K. Atreya, J. C. Stern, L. E. Christensen, T. Owen, H. Franz, R. O. Pepin, A. Steele; MSL Science Team, Isotope ratios of H, C, and O in CO₂ and H₂O of the Martian atmosphere. *Science* **341**, 260–263 (2013).
39. I. P. Wright, M. M. Grady, C. T. Pillinger, Chassigny and the nakhlites: Carbon-bearing components and their relationship to martian environmental conditions. *Geochim. Cosmochim. Acta* **56**, 817–826 (1992).
40. B. M. Jakosky, D. Brain, M. Chaffin, S. Curry, J. Deighan, J. Grebowski, J. Halekas, F. Leblanc, R. Lillis, J. G. Luhmann, L. Andersson, N. Andre, D. Andrews, D. Baird, D. Baker, J. Bell, M. Benna, D. Bhattacharyya, S. Bougher, C. Bowers, P. Chamberlin, J.-Y. Chaufray, J. Clarke, G. Collinson, M. Combi, J. Connerney, K. Connour, J. Correia, K. Crabb, F. Crary, T. Cravens, M. Crismani, G. Delory, R. Dewey, G. DiBraccio, C. Dong, Y. Dong, P. Dunn, H. Egan, M. Elrod, S. England, F. Eparvier, R. Ergun, A. Eriksson, T. Esmann, J. Espley, S. Evans, K. Fallows, X. Fang, M. Fillingim, C. Flynn, A. Fogle, C. Fowler, J. Fox, M. Fujimoto, P. Garnier, Z. Girazian, H. Groeller, J. Gruesbeck, O. Hamil, K. G. Hanley, T. Hara, Y. Harada, J. Hermann, M. Holmberg, G. Holsclaw, S. Houston, S. Inui, S. Jain, R. Jolitz, A. Kotova, T. Kuroda, D. Larson, Y. Lee, C. Lee, F. Lefevre, C. Lentz, D. Lo, R. Lugo, Y.-J. Ma, P. Mahaffy, M. L. Marquette, Y. Matsumoto, M. Mayyasi, C. Mazelle, W. McClintock, J. McFadden, A. Medvedev, M. Mendillo, K. Meziane, Z. Milby, D. Mitchell, R. Modolo, F. Montmessin, A. Nagy, H. Nakagawa, C. Narvaez, K. Olsen, D. Pawlowski, W. Peterson, A. Rahmati, K. Roeten, N. Romanelli, S. Ruhunusiri, C. Russell, S. Sakai, N. Schneider, K. Seki, R. Sharrar, S. Shaver, D. E. Siskind, M. Slipiski, Y. Soobiah, M. Steckiewicz, M. H. Stevens, I. Stewart, A. Stiepen, S. Stone, V. Tenishev, N. Terada, K. Terada, E. Thiemann, R. Tolson, G. Toth, J. Trovato, M. Vogt, T. Weber, P. Withers, S. Xu, R. Yelle, E. Yiğit, R. Zurek, Loss of the Martian atmosphere to space: Present-day loss rates determined from MAVEN observations and integrated loss through time. *Icarus* **315**, 146–157 (2018).
41. E. L. Scheller, B. L. Ehlmann, R. Hu, D. J. Adams, Y. L. Yung, Long-term drying of Mars by sequestration of ocean-scale volumes of water in the crust. *Science* **372**, 56–62 (2021).
42. R. J. Lillis, J. Deighan, J. L. Fox, S. W. Bougher, Y. Lee, M. R. Combi, T. E. Cravens, A. Rahmati, P. R. Mahaffy, M. Benna, M. K. Elrod, J. P. McFadden, R. E. Ergun, L. Andersson, C. M. Fowler, B. M. Jakosky, E. Thiemann, F. Eparvier, J. S. Halekas, F. Leblanc, J. Y. Chaufray, Photochemical escape of oxygen from Mars: First results from MAVEN in situ data. *J. Geophys. Res. Space Physics* **122**, 3815–3836 (2017).
43. S. W. Stone, R. V. Yelle, M. Benna, D. Y. Lo, M. K. Elrod, P. R. Mahaffy, Hydrogen escape from Mars is driven by seasonal and dust storm transport of water. *Science* **370**, 824–831 (2020).
44. M. S. Chaffin, D. M. Kass, S. Aoki, A. A. Fedorova, J. Deighan, K. Connour, N. G. Heavens, A. Kleinböhl, S. K. Jain, J. Y. Chaufray, M. Mayyasi, J. T. Clarke, A. I. F. Stewart, J. S. Evans, M. H. Stevens, W. E. McClintock, M. M. J. Crismani, G. M. Holsclaw, F. Lefevre, D. Y. Lo, F. Montmessin, N. M. Schneider, B. Jakosky, G. Villanueva, G. Liuzzi, F. Daerden, I. R. Thomas, J. J. Lopez-Moreno, M. R. Patel, G. Bellucci, B. Ristic, J. T. Erwin, A. C. Vandaele, A. Trokhimovskiy, O. I. Korablev, Martian water loss to space enhanced by regional dust storms. *Nat. Astron.* **5**, 1036–1042 (2021).
45. B. M. Jakosky, B. G. Henderson, M. T. Mellon, Chaotic obliquity and the nature of the Martian climate. *J. Geophys. Res. Planets* **100**, 1579–1584 (1995).
46. F. P. Wang, J. F. W. Gale, Screening criteria for shale-gas systems. *Gulf Coast Assoc. Soc. Transaction* **59**, 779–793 (2009).
47. T. Neill, D. Judd, E. Veith, D. Rousar, Practical uses of liquid methane in rocket engine applications. *Acta Astronaut.* **65**, 696–705 (2009).
48. C. Palmer, SpaceX starship lands on Earth, but manned missions to Mars will require more. *Engineering* **7**, 1345–1347 (2021).
49. R. M. Ramirez, R. Koppurapu, M. E. Zügger, T. D. Robinson, R. Freedman, J. F. Kasting, Warming early Mars with CO₂ and H₂. *Nat. Geosci.* **7**, 59–63 (2014).
50. B. M. Jakosky, C. S. Edwards, Inventory of CO₂ available for terraforming Mars. *Nat. Astron.* **2**, 634–639 (2018).
51. A. I. Oparin, The origin of life. (1953).
52. J. F. Kasting, D. Catling, Evolution of a habitable planet. *Annu. Rev. Astron. Astrophys.* **41**, 429–463 (2003).
53. W. C. Koeppen, V. E. Hamilton, Global distribution, composition, and abundance of olivine on the surface of Mars from thermal infrared data. *J. Geophys. Res. Planets* **113**, E05001 (2008).
54. C. Oze, M. Sharma, Have olivine, will gas: Serpentinization and the abiogenic production of methane on Mars. *Geophys. Res. Lett.* **32**, L10203 (2005).
55. D. Baratoux, H. Samuel, C. Michaut, M. J. Toplis, M. Monnereau, M. Wiczcok, R. Garcia, K. Kurita, Petrological constraints on the density of the Martian crust. *J. Geophys. Res. Planets* **119**, 1707–1727 (2014).
56. M. A. Wiczcok, A. Broquet, S. M. Mc Lennan, A. Rivoldini, M. Golombek, D. Antonangeli, C. Beghein, D. Giardini, T. Gudkova, S. Gyalay, C. L. Johnson, R. Joshi, D. Kim, S. D. King, B. Knapmeyer-Endrun, P. Lognonné, C. Michaut, A. Mittelholz, F. Nimmo, L. Ojha, M. P. Panning, A.-C. Plesa, M. A. Siegler, S. E. Smrekar, T. Spohn, W. B. Banerdt, InSight constraints on the global character of the Martian crust. *JGR Planets* **127**, 2022JE007298 (2022).
57. S. M. Clifford, The role of thermal vapor diffusion in the subsurface hydrologic evolution of Mars. *Geophys. Res. Lett.* **18**, 2055–2058 (1991).
58. L. Ji, T. Zhang, K. L. Milliken, J. Qu, X. Zhang, Experimental investigation of main controls to methane adsorption in clay-rich rocks. *Appl. Geochem.* **27**, 2533–2545 (2012).
59. M. J. Kennedy, S. C. Löhre, S. A. Fraser, E. T. Baruch, Direct evidence for organic carbon preservation as clay-organic nanocomposites in a Devonian black shale; from deposition to diagenesis. *Earth Planet. Sci. Lett.* **388**, 59–70 (2014).
60. G. Etiope, E. Ifandi, M. Nazzari, M. Procesi, B. Tsikouras, G. Ventura, A. Steele, R. Tardini, P. Szatmari, Widespread abiotic methane in chromitites. *Sci. Rep.* **8**, 8728 (2018).
61. G. Etiope, A. Ionescu, Low-temperature catalytic CO₂ hydrogenation with geological quantities of ruthenium: A possible abiotic CH₄ source in chromitite-rich serpentinized rocks. *Geofluids* **15**, 438–452 (2015).
62. M. W. Claire, J. Sheets, M. Cohen, I. Ribas, V. S. Meadows, D. C. Catling, The evolution of solar flux from 0.1 nm to 160 μm: quantitative estimates for planetary studies. *Astrophys. J.* **757**, 95 (2012).

Acknowledgments: We thank T. Bosak, B. Weiss, E. Scheller, and E. Kite for the insightful conversations on the topics of Martian mineralogy and atmospheric evolution. **Funding:** This work was supported by the National Science Foundation Division of Earth Sciences (NSF EAR), grant no. 1925863. **Author contributions:** J.M. was responsible for conceptualization, isotopic modeling, mineral thickness calculations, data compilation, data analysis, and writing. O.J. was responsible for conceptualization, data compilation, data analysis, and writing. **Competing interests:** The authors declare that they have no competing interests. **Data and materials availability:** All data needed to evaluate the conclusions in the paper are present in the paper and/or the Supplementary Materials.

Submitted 8 November 2023
 Accepted 21 August 2024
 Published 25 September 2024
 10.1126/sciadv.adm8443